

Time-lapse elastic full waveform inversion of CO₂ injection at CaMI FRS using VSP: a feasibility study

Ninoska Amundaray and Kris Innanen

ABSTRACT

Full waveform inversion (FWI) relies on the quality and frequency content of the data to recover subsurface models. Successful applications have proven to delimit reservoirs with high-resolution models, as well as, measuring parameter variations associated to production processes. Currently, an injection program of carbon dioxide (CO₂) is being conducted at the Containment and Monitoring Institute Field Research Station (CaMI.FRS). Field data from the baseline phase has been successfully inverted for the site, and data from an advanced injection stage is expected to be recorded in the following years. Hence, there is a need to assess the extents and limitations of this technique to resolve changes in the reservoir through experiments designs consistent with settings deployed at CaMI.FRS. In this study, we examine FWI using vertical seismic profiles (VSP) with velocity-density and impedance-velocity parameterizations, and by two inversion strategies in the data-space for three stages of CO₂ injection. Inverted models demonstrate superior constraints of P- and S-wave variations by a sequential inversion scheme in terms of relative change between modeled stages and model misfit. Likewise, impedance-velocity is suggested as the optimal parameterization to resolve reservoir changes with approximately 2% to 4% more measured variations.

INTRODUCTION

Full waveform inversion (FWI) is being thoroughly investigated for its capacity to provide tools for (1) high frequency model estimation in reservoir settings, and (2) short and long term monitoring of injection and other production processes, including carbon dioxide (CO₂) storage. FWI has been demonstrated both with simulations and field data to be very effective at producing high resolution P-wave velocity images of reservoirs, but the frequency content of data and the subtlety of the data variations associated with the above two applications will certainly stretch acquisition, computation, and algorithm-construction in FWI to its limits. The Containment and Monitoring Institute Field Research Station (CaMI.FRS) is a well-characterized test site perfectly designed to allow field scale testing of FWI in both of these capacities. Currently, CO₂ is being injected at the FRS (Macquet et al., 2019). In 2018, a large multi-offset and multi-azimuth VSP data set, including geophone and accelerometer data, and a broadband source, was acquired as a baseline for FWI studies (Hall et al., 2018); a comparable monitoring dataset is under development for acquisition in roughly one year. The baseline dataset is now beginning to produce elastic FWI results, using in-house CREWES frequency domain codes (Eaid et al., 2021; Keating et al., 2021). So, the question of whether, and how, a time-lapse signal should be expected to be resolvable with a monitoring FWI stage is currently a high priority. The purpose of this report is to discuss feasibility studies of elastic FWI in a time-lapse setting, using as realistic as possible, a set of parameters derived from the CaMI.FRS. It builds on the acoustic FWI studies presented last year by Amundaray et al. (2020).

An isotropic elastic description of the Earth's subsurface involves between one and three elastic constants, with that number shrinking if through prior information two or more constants are held to be correlated. The three basic constants are the compressional wave velocity (P-wave), shear wave velocity (S-wave) and density (ρ), which also relate to seismic waves at different wavelengths (i.e., short and long). Because FWI makes use of quite complicated relationships between information in data and model spaces, not all model parameterizations (i.e., parameters used to describe the subsurface) will produce the same solution. In fact, previous studies have demonstrated that selection of parameterization should be associated to the dataset utilized in the inversion (Tarantola, 1986; Mora, 1988; Pan et al., 2018). Particularly, for vertical seismic profiles (VSP), studies have shown that the dominance of transmitted waves help to recover velocity-density structures better than any other combination of elastic properties.

At CaMI.FRS, several technologies are being tested to examine a CO₂ injection in a clastic reservoir. VSP are amongst some of the surveys periodically recorded at this site to expand our understandings of carbon sequestration. Due to their fixed configuration, VSP tend to truthfully capture variations associated with reservoir properties, which make them suitable for CO₂ monitoring. Likewise, these surveys usually provide data with high signal-to-noise ratio that offer additional benefits for applications of FWI.

In this work, we study extent and constraints of elastic FWI for time-lapse analysis at CaMI.FRS. Here, we compared inversion results from two parameterizations during three stages of CO₂ injection proposed by Macquet et al. (2019). Although, initially we tested a simultaneous inversion in the data space, using the vertical and horizontal components of VSP. Our results indicate that a sequential inversion in the data space will improve the model convergence and the estimation of velocity changes associated to CO₂ at reservoir level.

FULL WAVEFORM INVERSION OF VSP DATA

In seismic, the recording of waves modes is governed by the acquisition design (i.e., sources and receiver locations). While reflection data tends to resolve better information from high wavenumbers, transmitted waves usually provide information associated to the low wavenumbers (Mora, 1988). Hence, it is important to analyze seismic inversion in terms of subsurface parameters and wave modes.

Wave components in VSP

In VSP surveys, seismic is usually acquired using three-component (3-C) geophones. This allows recording simultaneously P-waves and both polarised components of S-waves, SV-and SH-wave, in three directions. Though, it is commonly assumed that the vertical component of a VSP mostly comprises transmitted P-waves and the horizontal component registers reflections associated with P-and S-waves (Lu et al., 2019), in reality, both components have combined information about transmitted and reflected waves.

The quality of seismic data is usually associated with the amplitude and noise level in the recorded shots, which can be highly affected by phenomena related to subsurface

properties like layer effects, random scattering, geometric spreading, and others (Montano, 2017). Particularly in VSP, the amplitude of reflected waves is strongly affected by some of the mentioned effects. Contrary to transmitted waves, whose energy is better preserved due to the short distance traveled by direct waves. Hence, it is commonly said that VSP surveys are dominated by transmission events, even when both types of data coexist.

Model parameterization for VSP

To describe a perfectly elastic and isotropic medium, we need three parameters: density, and two Lamé constants known as λ and μ , or density, and P- and S-wave velocity. Although, in theory these are equivalent, the reconstruction of these constants from seismic will not yield the same results. The main reason behind this, it is the nonlinear relation between data and model parameters governed by wavelengths.

Several authors have qualitatively analyzed the resolution of subsurface parameters following the work of Tarantola (1986), using scattering radiation patterns. These ones provide information about the amplitude variations of elastic constants given by the opening angles of scattered wavefields, which are produced by medium perturbations. Because scattered wavefields are indistinct of parameters. We could have similar or overlapping patterns in a region that correspond to different elastic constants, which could lead to erroneous mapping in-between parameters and inversion of distorted structures. To minimize some of these undesirable features during inversion, it is recommended to consider: (1) the opening angles of seismic acquisition and (2) the expected parameter amplitude within those opening angles given a parameterization.

As mentioned before, VSP datasets comprise transmitted and reflected waves. Due to this, we are highly interested in two regions of scattering patterns. For the direct waves, we need to examine parameter resolution at wide angles (i.e., 135° to 225°); whereas, for reflection events we should inspect low angles. Using various combinations of elastic parameters, Pan et al. (2018) determined that velocity-density ($V_p - V_s - \rho$) parameterization reproduces the most reliable results from VSP. Likewise, Tarantola (1986) suggested that velocity-density parameterization is more appropriate for inversion data from large offset, and impedance-density is more suitable for near offset data. Additionally, Mora (1988) demonstrated that in VSP, transmitted waves will help to update the model in the initial iterations, and later, in late stage, reflections will give a boost in the resolution of fine-detailed velocity anomalies.

ELASTIC INVERSION OF VSP DATA AT CAMI FIELD RESEARCH STATION

Elastic models for CaMI.FRS

Macquet et al. (2019) modeled the elastic effects at reservoir level associated with a controlled injection of CO_2 at the Field Research Station. They suggested three distinct stages for the Basal Belly River Sandstone (BBRS), which is the primary reservoir. The first stage suggested is a baseline phase, prior to any gas injection, which is followed by a medium phase after 266 tons of CO_2 injected, and then, a final phase of injection after 1664 tons of CO_2 .

We used the projections for the site to construct the true models for density and P-wave velocity from 60 to 350 m depth. To estimate the missing information in shallow levels for the compressional wave velocity (i.e., first 60 m), we used an available VSP survey with values from surface to 324 m. Here, we picked the direct P-wave arrivals from near-offset shots. Then, we converted those values to velocity, and completed our P-wave model.

In the case of density at shallow depths, we estimated the parameters m and α from Gardner's relation given by:

$$\rho = \alpha V_p^m \quad (1)$$

After plotting density and velocity values between 60 to 350 m, and fitting a power regression. We obtained Equation 2 to calculate density:

$$\rho = 234V_p^{0.31} \quad (2)$$

For the shear wave velocity, we only had data for deep levels after 226 m. Hence, we plotted the available S- and P-wave data in a cross-plot, and estimated the parameters to adjust Castagna's relation based on our dataset. After fitting a polynomial of degree one, we obtained Equation 3 and estimated V_s from shallow levels using:

$$V_p = 1.1180V_s + 1391.9 \quad (3)$$

Figure 1 shows the linear and power regression estimated for this investigation. Whereas, Figure 2 displays a profile view from our constructed models for density and velocities at the baseline phase, using well-logs, previous studies and empirical relationships. Overlaid on the previous image, there is a smoothed versions of each model. They were obtained using a Gaussian smoother with a half-width of 5 m, to maintain the balance between seismic and model resolution. These smoothed versions were used as true models during the inversion process; hence, they will be referred as so, in the upcoming analysis.

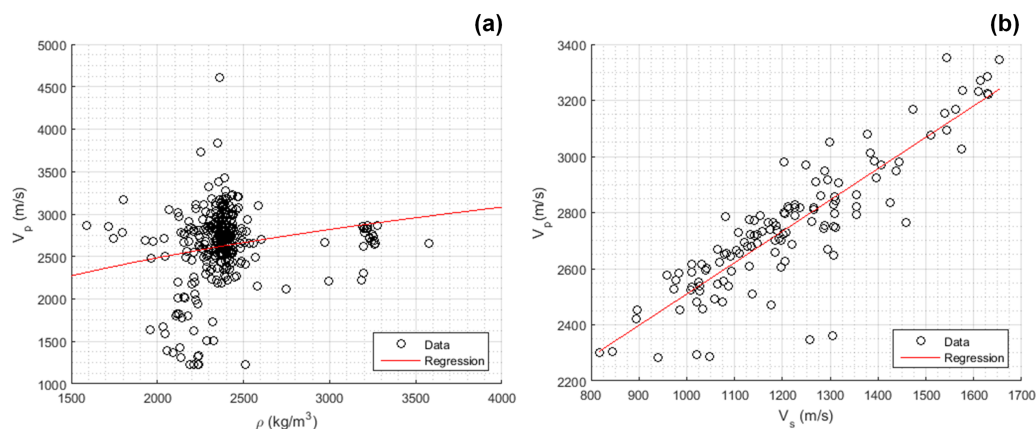


FIG. 1. Cross-plots of available information at CaMI FRS with the estimated regression models. (a) Power regression from P-wave and density between 60 to 350 m depth, and (b) linear regression from P- and S-wave between 266 to 350 m depth.

Figure 3 and Figure 4 show the true and initial models considered in this investigation. A grid cell size of 5 x 5 m was defined in the horizontal and vertical scale, with a maximum

horizontal and vertical distance of 1000 m and 350 m, respectively. The initial model for all simulated stages at the FRS was a smoothed version of the baseline phase that was estimated by Gaussian smoother with a half-width of 25 m.

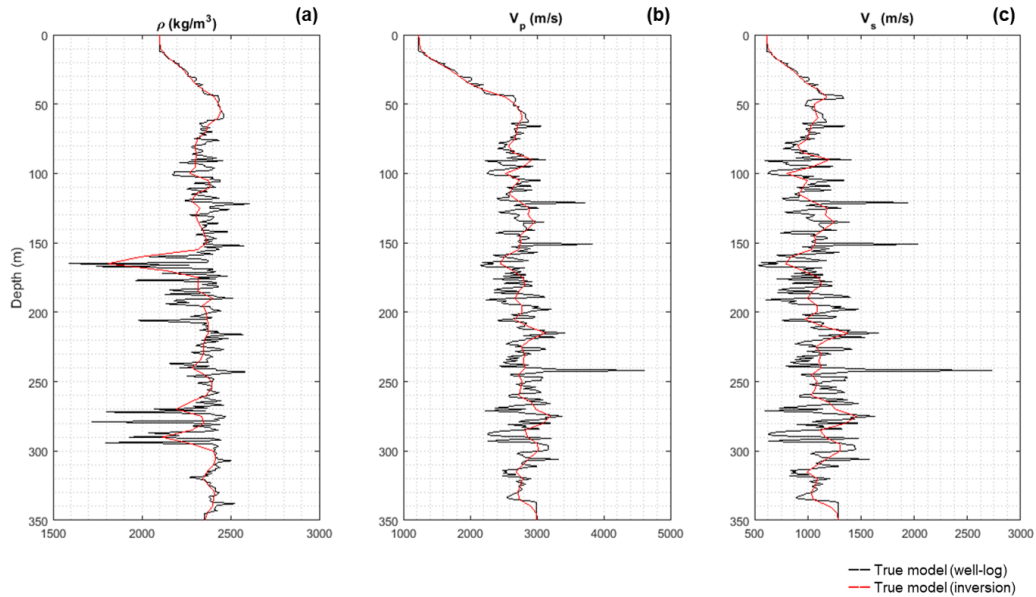


FIG. 2. True models constructed for this investigation. Where (a) is the density, (b) P-wave velocity, and (c) S-wave velocity. In the three panels, black lines are based on well-log information and red lines are a smoothed version from well-logs.

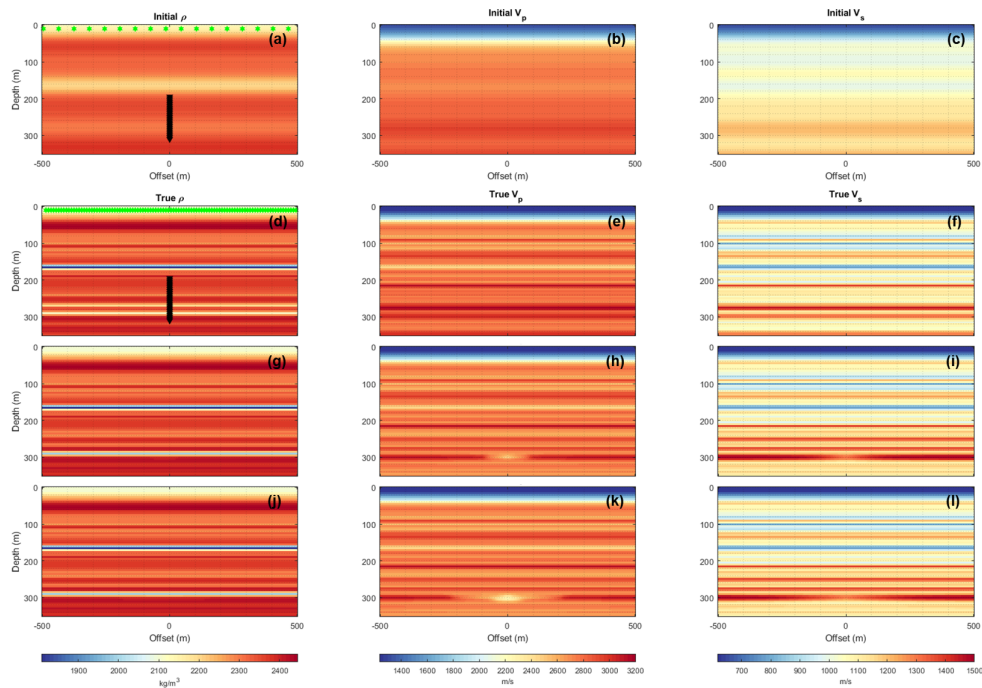


FIG. 3. Initial and true models for $V_p - V_s - \rho$ parameterization for three phases of CO_2 injection. (a)-(c) are the initial models for all stages, (d)-(f) are the baseline models, (g)-(i) are models from a medium phase injection after 266 CO_2 , and (j)-(l) are models from the final phase of injection after 1666 CO_2 . Green markers represent source locations, and black triangles indicate the receivers, which were located in the observation well at zero-offset.

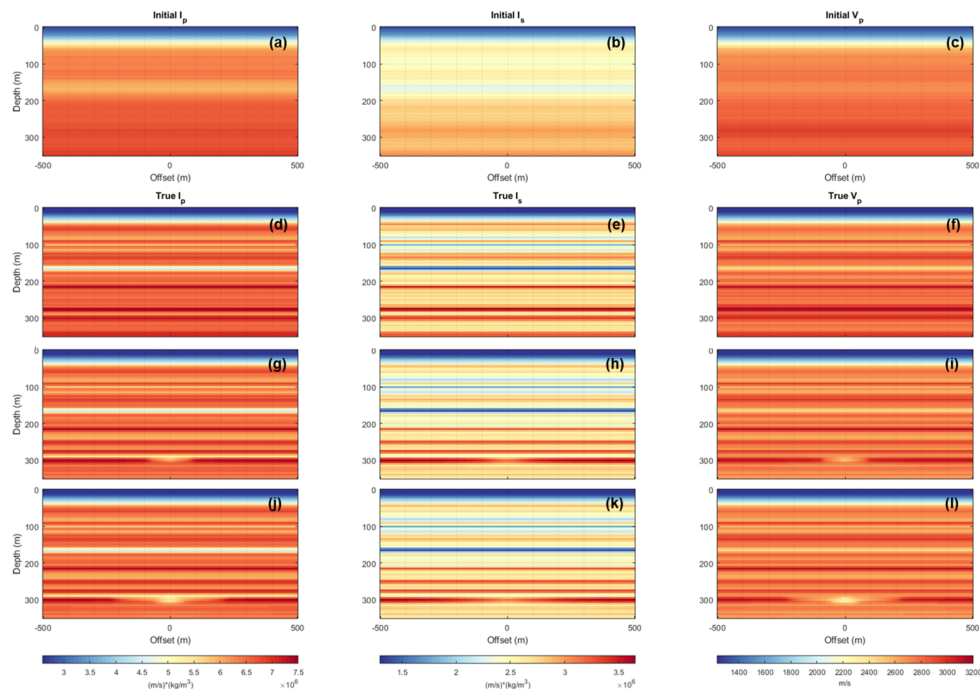


FIG. 4. Initial and true models for $I_p - I_s - V_p$ parameterization for three phases of CO_2 injection. (a)-(c) are the initial models for all stages, (d)-(f) are the baseline models, (g)-(i) are models from a medium phase injection after 266 CO_2 , and (j)-(l) are models from the final phase of injection after 1666 CO_2 . The observation well for VSP simulation is located in the center of the models, at zero-offset.

Modeled VSP experiments

For modeling synthetic data, we used a frequency domain full waveform inversion algorithm based on finite-difference approximation. We simulated the permanent acquisition design at the FRS with a disposition of vertical receivers separated every 5 m between 190 to 305 m. Likewise, we considered two source distributions with a separation of 60 m and 10 m, as shown in Figure 3(a) and 3(d). Where, the former represents the regular distance utilized at the site to record VSP, and the second was a source spacing tested during an one-time VSP experiment carried out by CREWES in 2018 (Hall et al., 2018). In a previous acoustic study for this site (Amundaray et al., 2020), it was observed that the resolution of subsurface properties is mostly controlled by number of modeled sources and not the receiver disposition. Therefore, we are not underestimating our model resolution by using a single receiver arrangement.

Explosive sources were considered in this study and located on the surface. Sources were simulated with thirteen frequency bands from [4-6 Hz], to [4-8 Hz], [4-10 Hz], [4-12 Hz], [4-14 Hz], [4-16 Hz], [4-18 Hz], [4-20 Hz], [4-22 Hz], [4-24 Hz], [4-26 Hz], [4-28 Hz], and [4-30 Hz], where each band consisted of fifteen evenly separated frequencies.

Inversion scheme

Based on results from previous investigations, two parameterizations are suggested for inversion of VSP datasets. We used both, velocity-density ($V_p - V_s - \rho$) and impedance-

velocity ($I_p - I_s - V_p$), to invert model properties simultaneously from three phases of CO₂ injection. After initial results, we observed that density structures displayed significant cross-talk (i.e., erroneous mapping between parameters); thus, we did not invert it directly. Nonetheless, we simulated density effects through impedance, when using $I_p - I_s - V_p$ parameterization, and by fixing density to an initial value in $V_p - V_s - \rho$ parameterization in an effort to characterize the true model response captured by seismic. Yet, as demonstrated by Macquet et al. (2019), CO₂ variations are not expected to affect significantly density, as much as, P- and S-wave velocities. Hence, our biggest focus during the inversion was to constraint velocity structures.

To exploit the benefits of VSP (i.e., presence of transmission and reflection events), we examined two inversion strategies in the data space. Firstly, we utilized both, vertical and horizontal components of the survey simultaneously, and invert for subsurface properties. Secondly, we defined a sequential inversion. For this one, we only utilized the vertical component of VSP when inverting for low frequencies, and then, incorporated the horizontal component information when using low-medium frequencies.

Lastly, model convergence was assessed in each test by normalizing the residuals within 190 to 325 m (i.e., effective depths inverted in our investigation) with Equation 6:

$$residual_i = \frac{1}{N} \sum_{k=1}^N (true_i - observed_i)^2 \quad (4)$$

$$norm_i = \frac{1}{N} \sum_{k=1}^N (true_i - initial_i)^2 \quad (5)$$

$$model_residual_i = \frac{residual_i}{norm_i} \quad (6)$$

Where the suffix i is the injection phase, $true$ refers to the true model, $observed$ is the inverted model, $initial$ refers to the initial model, and N is the number of samples.

RESULTS

In this study, all inverted models were slightly regularized to diminish the artifacts associated with the source footprint. Here, the regularization term enforces a level of smoothness and lateral continuity, suitable for “layer-cake” models, as it is the geology at CaMIFRS. If not regularization is used, inverted models will still resolve horizontal layers but with the addition of fabricated patterns.

Inversion results using multicomponent data simultaneously are shown in Figure 5 and Figure 6, for velocity-density and impedance-velocity parameterizations, respectively. In both cases, the last frequency band, that was reliably inverted, was [4-26 Hz]. After this, model updates mostly introduced artifacts that diminished the lateral continuity of the inverted parameters. At reservoir level, all inverted models converged towards the true solution with minor variations in the resolution of the CO₂ plume. Though, the vertical extend of this is fully captured using either, $V_p - V_s - \rho$ and $I_p - I_s - V_p$, as parameterization; the

lateral extension is better resolved by $I_p - I_s - V_p$, which is most likely associated by the relation that each parameter has with spatial wavelengths.

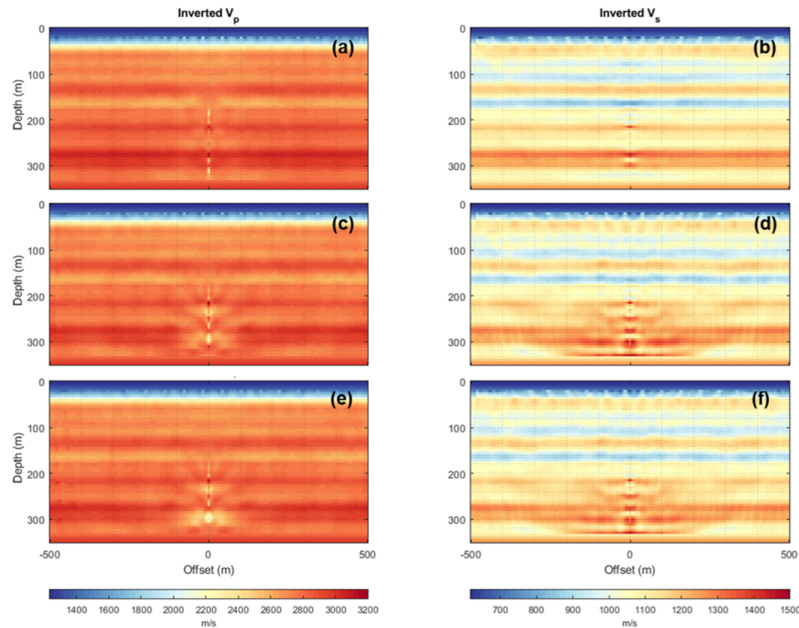


FIG. 5. Inverted models for three phases of CO₂ injection using multicomponent VSP data simultaneously with $V_p - V_s - \rho$ parameterization and 60 m source spacing. (a)-(b) are the the inverted baseline models, (c)-(d) are the inverted medium phase models, and (e)-(f) are the inverted final phase models.

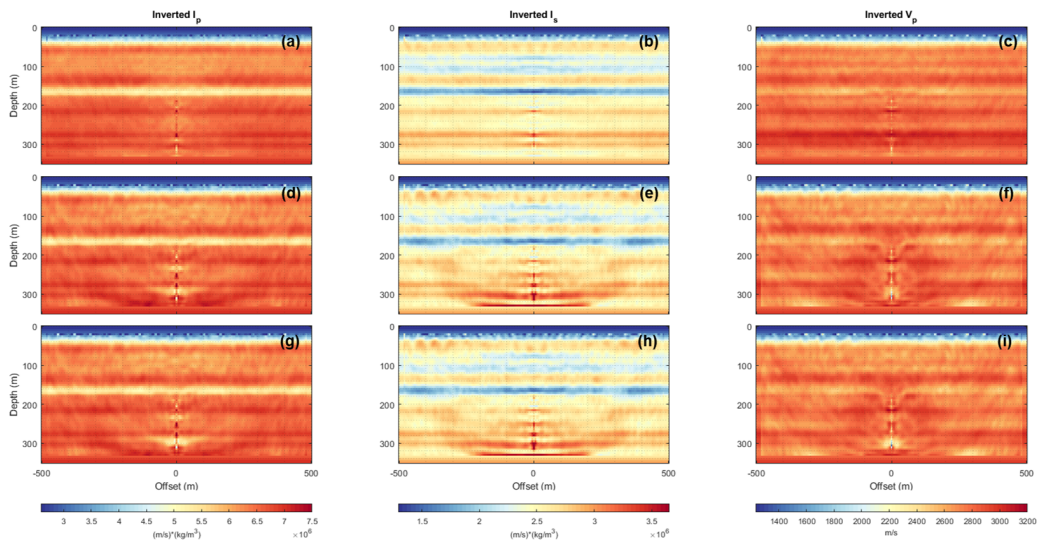


FIG. 6. Inverted models for three phases of CO₂ injection using multicomponent VSP data simultaneously with $I_p - I_s - V_p$ parameterization and 60 m source spacing. (a)-(c) are the inverted baseline models, (d)-(f) are the inverted medium phase models, and (g)-(i) are the inverted final phase models.

After positive observations using a 60 m source distribution, we tested the effects of increasing the number of sources, similarly to a previous experiment at the FRS. Impedance-

velocity parameterization was utilized to exploit the definition of CO₂ effects laterally with additional data. As Figure 7 shows, model updates are observable within a 300 m radius from the observation well located at zero offset at different levels. This value represents an increment of 150% from the effective distance resolved in the previous experiments. As it can be expected, introduction of sources led to stronger artifacts by source footprint. Because regularization terms were not properly tuned for this case, direct comparison of model residuals with different source spacing should be avoided as reference.

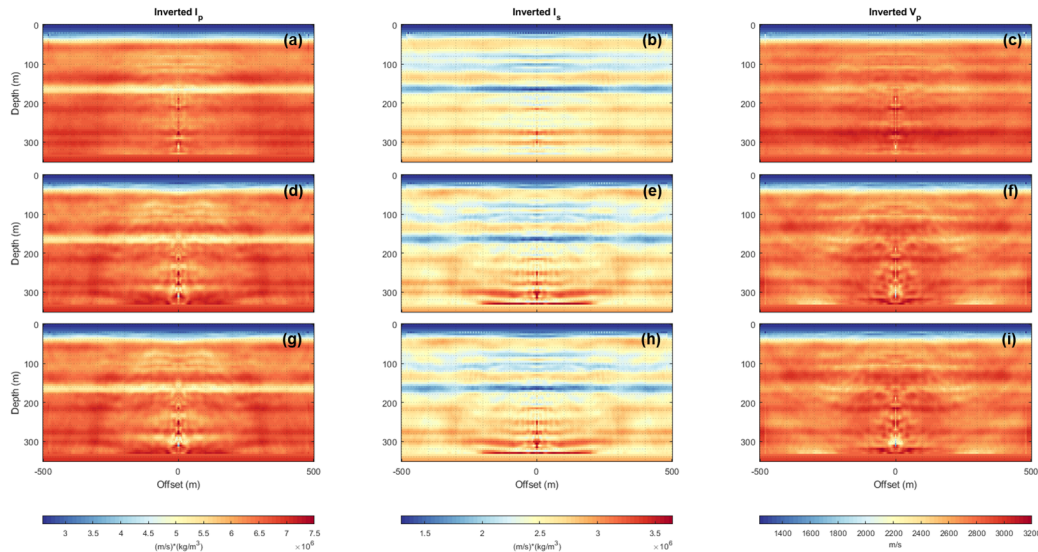


FIG. 7. Inverted models for three phases of CO₂ injection using multicomponent VSP data simultaneously with $I_p - I_s - V_p$ parameterization and 10 m source spacing. (a)-(c) are the inverted baseline models, (d)-(f) are the inverted medium phase models, and (g)-(i) are the inverted final phase models.

Figure 8 and Figure 9 follow a sequential inversion at two frequency bands for both parameterizations. Models from band [4-24 Hz] were inverted using only the vertical component from synthetic VSP; while, models from band [4-30 Hz] were obtained inverting multicomponent data simultaneously. Results from this scheme demonstrate that model parameters are satisfied differently by wavenumbers and wave modes. While large-scaled structures can be resolved using, mostly, seismic data provided by direct waves in the vertical component. Fine-detailed structures benefit from reflection events that are abundant in the horizontal component of VSP. As Figure 8(e), 8(g), 8(i), 8(k) and Figure 9(g), 9(j), 9(m), 9(p) show, the lateral and vertical extension of the CO₂ effects were resolved better, once we introduce multicomponent data.

In Figure 10, Figure 11, Figure 12 and Figure 13, we display the velocity profiles for P- and S-wave from the three modeled stages of CO₂ injection. For reference, the near offset profile is located at 20 m from the receiver arrangement; whereas, the far offset is set at 120 m. Velocity structures from impedance were reconstructed because we are interested in direct comparison between inverted models. At reservoir level (around 300 m), we can identify variations associated to the expected gas injection. In all cases, there is a progressive reduction of P-wave velocity from the baseline to the final phase, as well as, an increment in the S-wave velocity at the same depths. Nonetheless, it appears that

these changes are inversely proportional between each other. With increasing offset, P-wave variations tend to be attenuated; whereas S-wave effects increase. This follows the predictions from the true models for the first parameter, but not entirely for the second one. According to our models, variations in the shear wave are not very distinguishable between injection stages, but when they do occur, they seem to follow the same decreasing trend like P-wave.

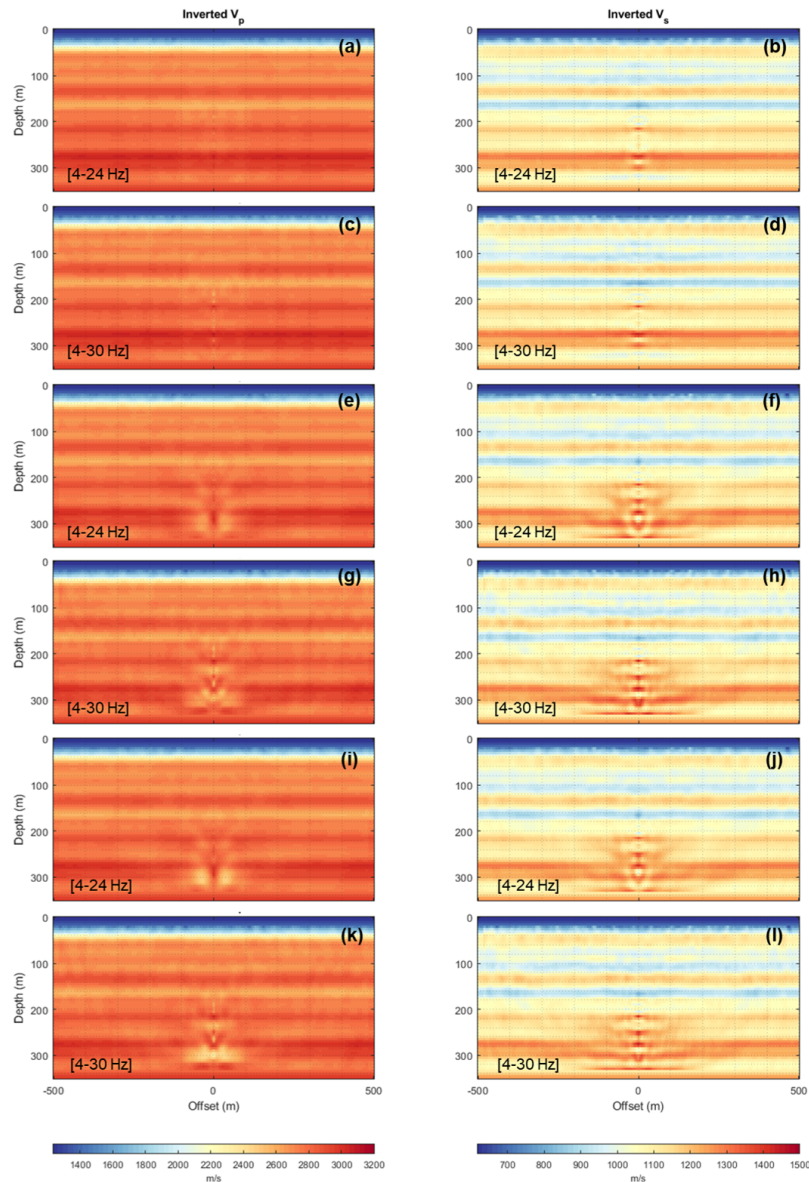


FIG. 8. Inverted models from two frequency bands for three phases of CO₂ injection using a sequential inversion strategy with $V_p - V_s - \rho$ parameterization. (a)-(d) are the inverted baseline models (e)-(h) are the inverted medium phase models, and (i)-(l) are the inverted final phase models.

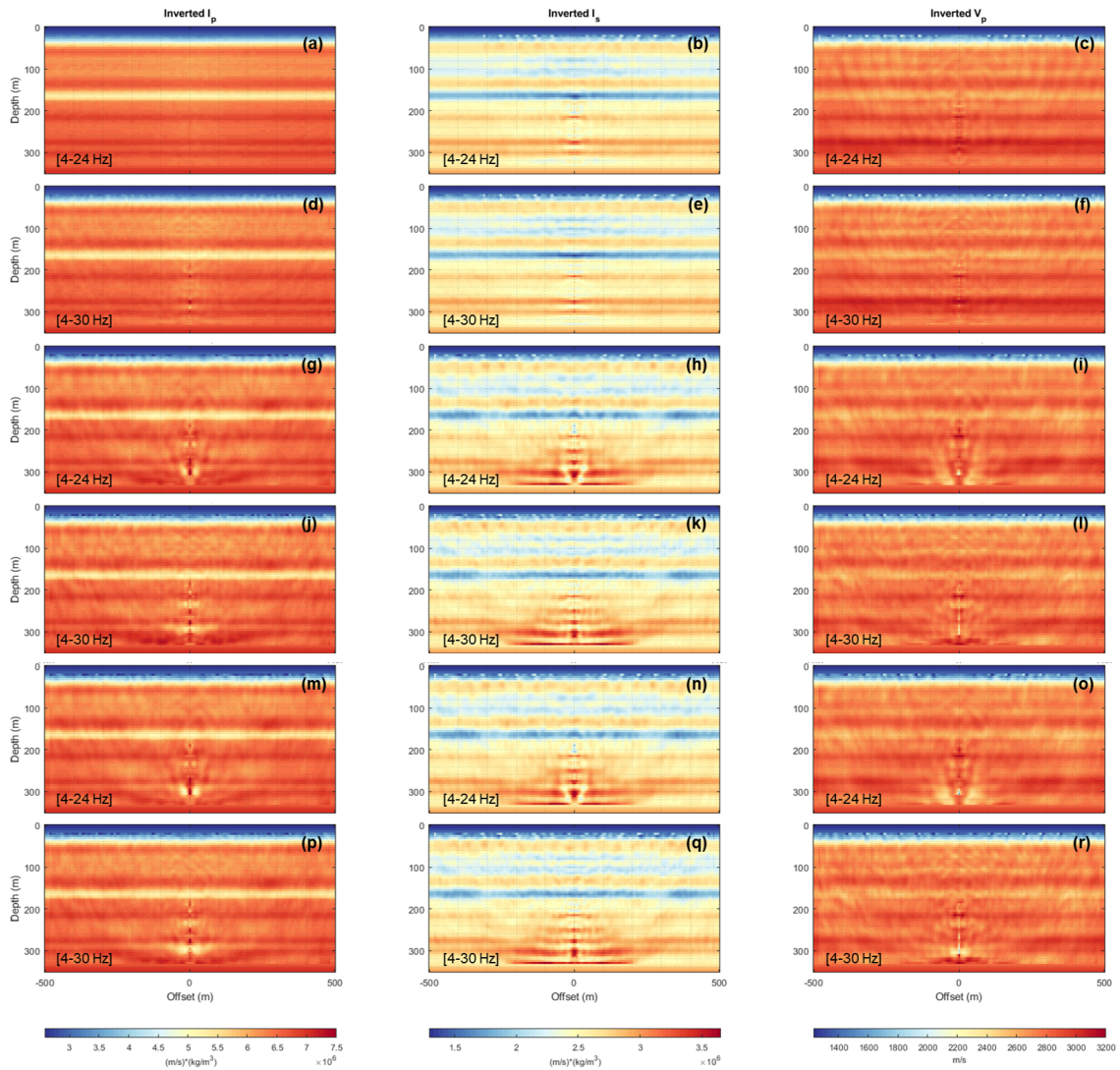


FIG. 9. Inverted models from two frequency bands for three phases of CO_2 injection using a sequential inversion strategy with $I_p - I_s - V_p$ parameterization. (a)-(f) are the inverted baseline models, (g)-(l) are the inverted medium phase models, and (m)-(r) are the inverted final phase models.

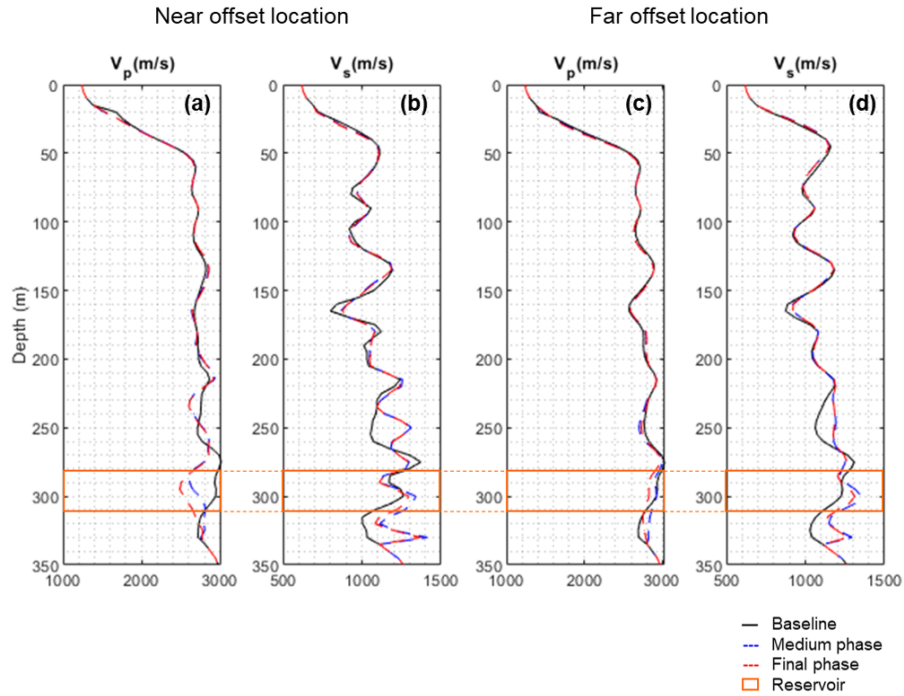


FIG. 10. Profile views from inverted models using multicomponent data simultaneously and $V_p - V_s - \rho$ as parameterization at two offset locations. (a)-(b) are located at 20 m from the observation well, and (c)-(d) are located at 120 m from the observation well. In these four panels black lines are the inverted baseline, blue dashed lines are the inverted medium phase, red dashed lines are the inverted final phase, and orange boxes indicate the reservoir.

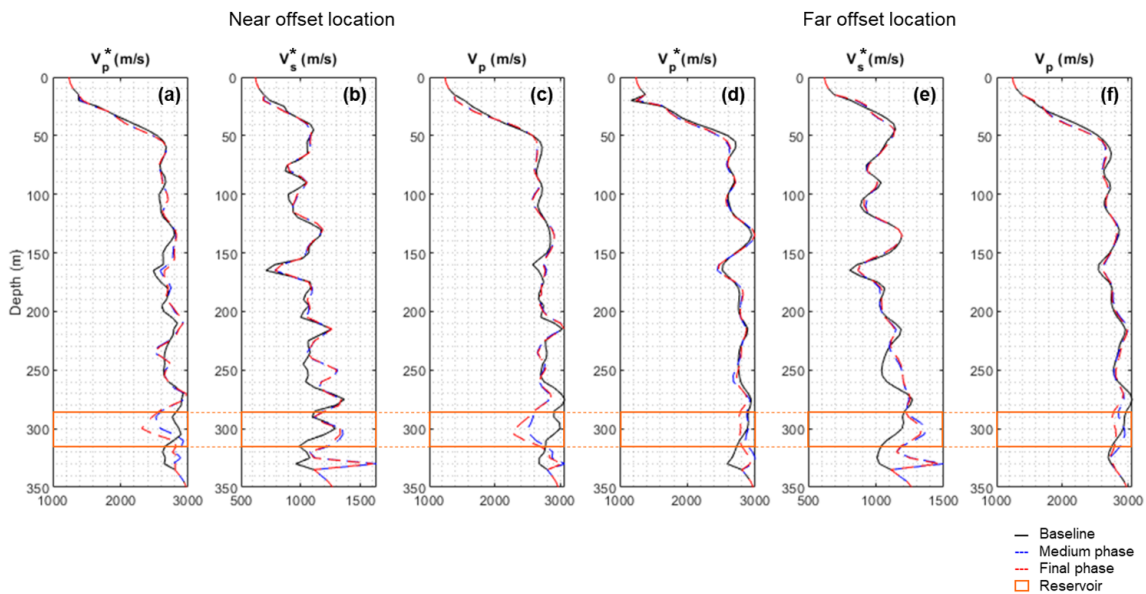


FIG. 11. Profile views from inverted models using multicomponent data simultaneously and $I_p - I_s - V_p$ as parameterization at two offset locations. (a)-(c) are located at 20 m from the observation well, and (d)-(f) are located at 120 m from the observation well. In the six panels black lines are the inverted baseline, blue dashed lines are the inverted medium phase, red dashed lines are the inverted final phase, and orange boxes indicate the reservoir. Asterisks on top of V_p and V_s refer to velocities reconstructed from impedance.

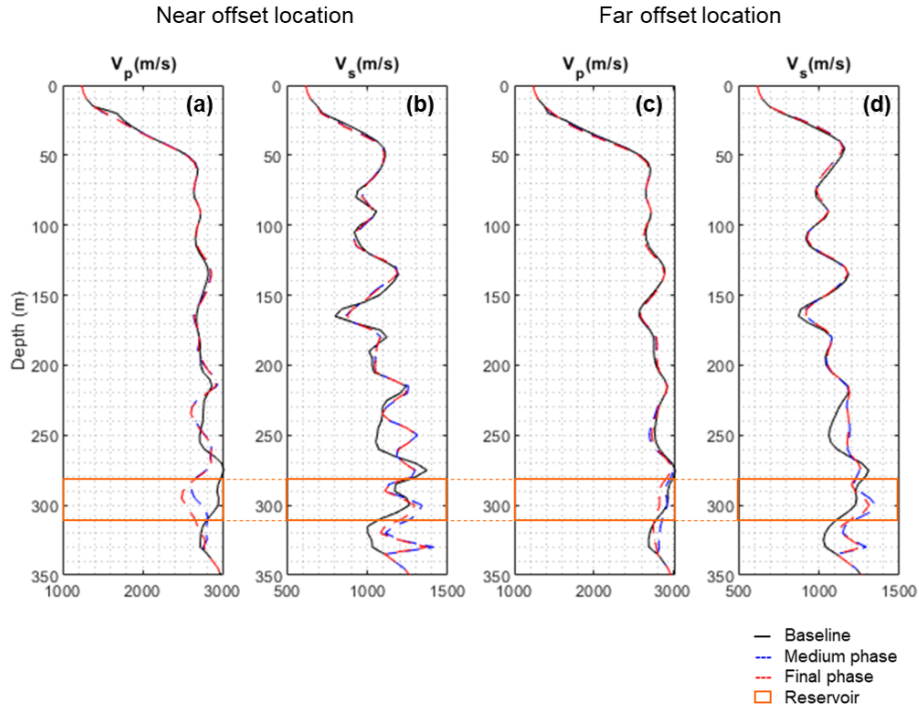


FIG. 12. Profile views from inverted models using a sequential inversion strategy and $V_p - V_s - \rho$ as parameterization at two offset locations. (a)-(b) are located at 20 m from the observation well, and (c)-(d) are located at 120 m from the observation well. In these three panels black lines are the inverted baseline, blue dashed lines are the inverted medium phase, red dashed lines are the inverted final phase, and orange boxes indicate the reservoir.

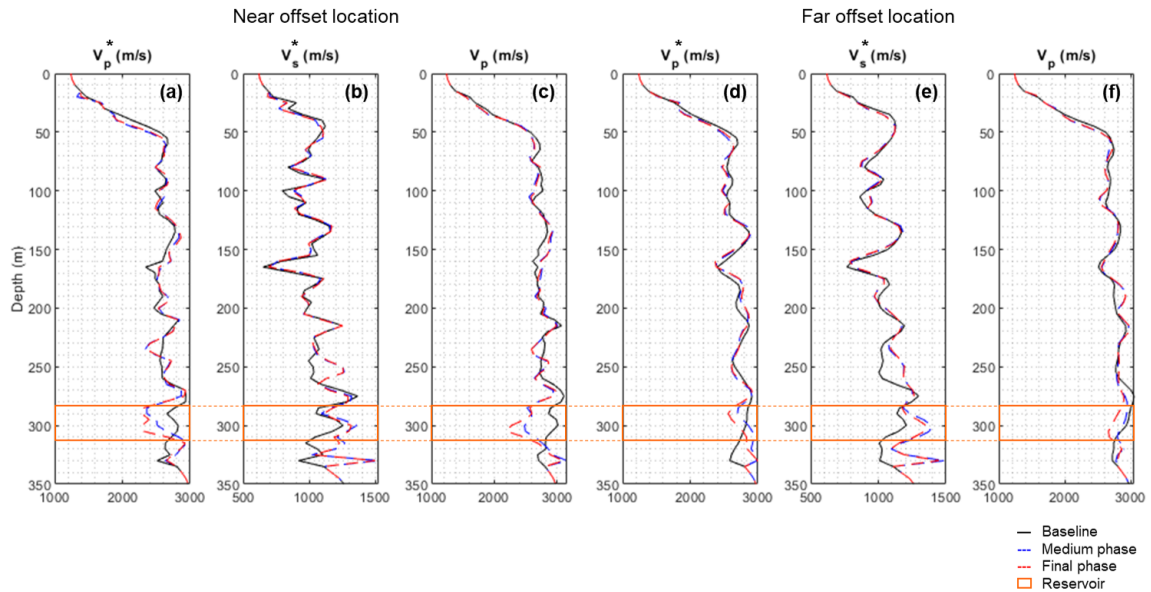


FIG. 13. Profile views from inverted models using sequential inversion strategy and $I_p - I_s - V_p$ as parameterization at two offset locations. (a)-(c) are located at 20 m from the observation well, and (d)-(f) are located at 120 m from the observation well. In the six panels black lines are the inverted baseline, blue dashed lines are the inverted medium phase, red dashed lines are the inverted final phase, and orange boxes indicate the reservoir. Asterisks on top of V_p and V_s refer to velocities reconstructed from impedance.

As seen thoroughly in the velocity profiles, variations in the models are mostly registered between 190 to 330 m, which correlates with the location of receivers in experiment. Bottom values after 315 m exhibit large spikes that should be regarded as artifacts made by the algorithm, while trying to approximate the edges of the model. Although the reservoir thickness is about 7 m, deflections associated to the CO₂ effects appear within 290 to 305 m depth in all inverted models. This gives a total thickness of 15 m to the BBRS, which is about twice its real value. But understandably, the true thickness of this reservoir is not very likely to be resolved by seismic methods. Likewise, we observe more perturbations along the profiles in-between stages for S-wave structures than in P-wave. Nonetheless, as estimated metrics from Table 2 and Table 3 show, model residuals from each parameter are similar at some injection phases. Hence, we cannot suggest one parameter as more reliable than other.

Comparison of model residuals in Table 2 and Table 3 indicates that a sequential inversion of multicomponent data led to a superior convergence in the three simulated phases. This remark is independent of the parameterization used. Although, it should be noticed that lower levels of model residuals are obtained with velocity-density parameterization because this one exploits more the usage of transmission events that dominates VSP. Hence, if the inversion objective is assessing the definition of model structures, this should be considered as the optimal option. Because our primary target is evaluating FWI as a technique for reservoir monitoring in a CO₂ sequestration program. We are concerned with measuring variations in the reservoir and not just the definition of subsurface structures. As seen in Table 1, Table 2, and Table 3, larger parameter variations were estimated when we employed the impedance-velocity parameterization, due to the tendency of reflection events to resolve sudden variations of P- and S-wave velocity.

Table 1. Summary of inversion results with $I_p - I_s - V_p$ parameterization using multicomponent data simultaneously, which were modeled with a source spacing of 10 m. V_p^* and V_s^* indicate velocities reconstructed from impedance.

Parameterization	Parameter	Injection phase	Model residuals	Parameter variation(%)	
				Near Offset	Far Offset
$I_p - I_s - V_p$	$I_p \rightarrow V_p^*$	Baseline	1.5357	0.00	0.00
	$I_s \rightarrow V_s^*$		1.0338	0.00	0.00
	V_p		1.0959	0.00	0.00
	$I_p \rightarrow V_p^*$	Medium	0.9997	-10.68	4.94
	$I_s \rightarrow V_s^*$		0.8353	8.32	15.60
	V_p		0.9732	-17.66	-3.82
	$I_p \rightarrow V_p^*$	Final	0.8399	-18.60	-9.79
	$I_s \rightarrow V_s^*$		0.8922	4.98	12.07
	V_p		0.7595	-24.62	-10.45

As mentioned, the largest change of P-wave was measured at near offset locations with a

maximum of 24% and 21% when using a source distribution of 10 m and 60 m, respectively. S-wave velocity variations are more difficult to interpret. Though, they appear to increase with offset, they do not follow a trend like P-waves. In several cases, S-wave values are greater at a medium phase of CO₂ injection, and then, they decrease at a late phase. Only when a sequential inversion strategy is used, we were able to measure a reduction of this parameter. From time-lapse analyses, we observe that our proposed sequential scheme help us to estimate greater changes in the reservoir. We able to measure an extra 2% and 4% of changes with density-velocity and impedance-velocity parametrization, once results were compared with the simultaneous inversion of multicomponent data.

Table 2. Summary of inversion results per parameterization using multicomponent data simultaneously, which were modeled with a source spacing of 60 m. V_p^* and V_s^* indicate velocities reconstructed from impedance.

Parameterization	Parameter	Injection phase	Model residuals	Parameter variation(%)	
				Near Offset	Far Offset
$V_p - V_s - \rho$	V_p	Baseline	1.0785	0.00	0.00
	V_s		0.9279	0.00	0.00
	ρ				
	V_p	Medium	0.7905	-10.89	-1.03
	V_s		0.7862	2.52	7.05
	ρ				
	V_p	Final	0.6429	-15.18	-3.55
	V_2		0.8143	6.02	10.29
	ρ				
$I_p - I_s - V_p$	$I_p \rightarrow V_p^*$	Baseline	1.2040	0.00	0.00
	$I_s \rightarrow V_s^*$		0.9731	0.00	0.00
	V_p		1.0063	0.00	0.00
	$I_p \rightarrow V_p^*$	Medium	0.9326	-9.41	0.49
	$I_s \rightarrow V_s^*$		0.8390	4.51	15.10
	V_p		0.8942	-16.39	-1.43
	$I_p \rightarrow V_p^*$	Final	0.7805	-17.56	-3.29
	$I_s \rightarrow V_s^*$		0.8642	3.03	12.25
	V_p		0.7109	-22.98	-4.57

Table 3. Summary of inversion results per parameterization using a sequential inversion scheme, which were modeled with a source spacing of 60 m. V_p^* and V_s^* indicate velocities reconstructed from impedance.

Parameterization	Parameter	Injection phase	Model residuals	Parameter variation(%)	
				Near Offset	Far Offset
$V_p - V_s - \rho$	V_p	Baseline	1.0110	0.00	0.00
	V_s		0.9072	0.00	0.00
	ρ				
	V_p	Medium	0.7640	-12.49	-1.80
	V_s		0.8061	2.19	6.42
	ρ				
	V_p	Final	0.6113	-16.41	-5.34
	V_s		0.8151	3.45	8.86
	ρ				
$I_p - I_s - V_p$	$I_p \rightarrow V_p^*$	Baseline	1.1110	0.00	0.00
	$I_s \rightarrow V_s^*$		0.9120	0.00	0.00
	V_p		0.9538	0.00	0.00
	$I_p \rightarrow V_p^*$	Medium	0.8862	-13.25	-1.55
	$I_s \rightarrow V_s^*$		0.7982	-1.26	16.24
	V_p		0.7576	-11.52	-1.26
	$I_p \rightarrow V_p^*$	Final	0.7376	-21.22	-4.78
	$I_s \rightarrow V_s^*$		0.8254	-1.26	14.11
	V_p		0.6130	-20.77	-5.19

CONCLUSIONS

Two elastic full waveform inversion schemes were investigated with synthetic VSP data from CaMI.FRS at three stages of CO₂ injection. At reservoir level, inverted models demonstrate lateral and vertical resolution of the gas effects in P- and S-wave structures using velocity-density and impedance-velocity parameterization. Density properties were simulated but not directly inverted in this study, due to significant cross-talk associated to this parameter. Sequential inversion of multicomponent data showed superior constraints of velocity structures and allowed the implementation of higher frequency bands with less artifacts produced by source footprint. Time-lapse analysis indicates a maximum decrease of 24% and 21% in P-wave velocity with a source spacing of 10 m and 60 m, respectively, in the final stage of CO₂ injection at near offset location defined at 20 m from the observation well. S-wave velocity changes are inconclusive because values increases and decreases without following a particular pattern. In every test, impedance-velocity parameterization allowed us measure greater changes at reservoir level associated to CO₂ effects. We registered between 4% and 2% more variations in our inverted velocity with impedance-

velocity. Although, normalized model residuals suggest a better model convergence when using velocity-density parameterization.

ACKNOWLEDGEMENTS

We thank the sponsors of CREWES for continued support. This work was funded by CREWES industrial sponsors and NSERC (Natural Science and Engineering Research Council of Canada) through the grant CRDPJ 543578-19. We also acknowledge the Containment and Monitoring Institute for providing critical information for this investigation. Likewise, we thank Scott Keating for the assistance provided during the implementation of his FWI codes.

REFERENCES

- Amundaray, N., Innanen, K. A. H., Macquet, M., and Lawton, D. C., 2020, FWI time-lapse monitoring of CO₂ injection using VSP at CaMI FRS: a feasibility study: CREWES Research Report, **32**, No. 2.
- Eaid, M., Keating, S., and Innanen, K. A. H., 2021, Full waveform inversion of das field data from the 2018 cami vsp survey: CREWES Research Report, **33**, No. 6.
- Hall, K. W., Bertram, K. L., Bertram, M. B., Innanen, K. A. H., and Lawton, D. C., 2018, CREWES 2018 multi-azimuth walk-away VSP field experiment: CREWES Research Report, **30**, No. 16.
- Keating, S., Eaid, M., and Innanen, K. A. H., 2021, Full waveform inversion of vsp accelerometer data from the cami field site: CREWES Research Report, **33**, No. 28.
- Lu, J., Wang, Y., Chen, J., and Sun, P., 2019, P- and s-mode separation of three-component vsp data: Exploration Geophysics, **50**, No. 4, 430–448.
- Macquet, M., Lawton, D. C., Saeedfar, A., and Osadetz, K. G., 2019, A feasibility study for detection for detections thresholds of co₂ at shallow depths at the cami field research station, newell county, alberta, canada: Petroleum Geoscience, **25**, No. 4, 509–518.
- Montano, M., 2017, Seismic attenuation measurements from multicomponent vertical seismic profile data: M.Sc. thesis, Univ. of Calgary.
- Mora, P., 1988, Elastic wave-field inversion of reflection and transmission data: Geophysics, **53**, No. 6, 750–759.
- Pan, W., Innanen, K. A., and Geng, Y., 2018, Elastic full-waveform inversion and parametrization analysis applied to walk-away vertical seismic profile data for unconventional (heavy oil) reservoir characterization: Geophysical Journal International, **213**, No. 3, 1934–1968.
- Tarantola, A., 1986, A strategy for nonlinear elastic inversion of seismic reflection data: Geophysics, **51**, No. 10, 1893–1903.